Instability due to double-diffusive phenomenon in pressure-driven displacement flow of one fluid by another in an axisymmetric pipe

Kunal Dilip Bhagat, Manoj Kumar Tripathi, Kirti Chandra Sahu[1]

Department of Chemical Engineering, Indian Institute of Technology Hyderabad, Yeddumailaram 502 205, Telangana, India

Abstract

The pressure-driven displacement flow of a less viscous fluid initially occupying an axisymmetric pipe by a highly viscous fluid is investigated. The fluids consist of two species diffusing at different rates. The fluids are assumed to be Newtonian, incompressible with the same density, but different viscosity modelled as an exponential function of the concentration of both the species. A parametric study investigating the effects of diffusivity ratio, log-mobility ratios of the slower and faster diffusing species and Reynolds number on the flow dynamics is conducted. Our results demonstrate the presence of instability patterns due to double-diffusive effect in situations when a less viscous fluid displaces a highly viscous fluid. These instabilities are qualitatively different from those observed in planar channel. The intensity of these instabilities increases with increasing the values of diffusivity ratio. It is demonstrated that a highly viscous stenosis region is created near the entrance of the pipe due to double-diffusive effect, providing a favourable condition to start the instability. In addition to this, because of double-diffusive effect locally at some portion of the pipe, the less viscous fluid becomes the displacing fluid, which promotes the development of instability.

Keywords: Laminar flow, Mixing, CFD, Double-diffusive effect, Instability, Multiphase flow

[1]Email: ksahu@iith.ac.in

1. Introduction

The viscous fingering phenomenon in the displacement flows of a highly viscous fluid by a less viscous one has been widely studied in literature due to its relevance in many industrial applications and natural phenomena [1]. It is also well known that the opposite situation, wherein a less viscous fluid is displaced by a highly viscous one is stable [2–6]. However, these conclusions are only true for "single-component" systems, where viscosity stratification is achieved by varying one species, say temperature or concentration. Recently, it was observed that the classically stable viscosity-stratified configurations in the context of single-component flows become unstable in the presence of two species having different diffusion constants (say, temperature and salt, or sugar and salt, etc) in porous media [7], and pressure-driven flows in two-dimensional planar channel [8–13]. This phenomenon is commonly known as "double-diffusive" effect, which has been extensively studied in *density-stratified* systems (see for example Turner [14]), but has received far less attention in *viscosity-stratified* flows. Moreover, to the best of our knowledge, all the previous studies are conducted for planar geometries, although in most of the industrial applications the geometries are circular in cross section. **The flow dynamics in a circular pipe are very different to those of the planar channel**, as far as the instability and transition to turbulence are concerned [15]. Thus, the focus of the present study is to investigate the instability patterns due to the double-diffusion phenomenon in an axisymmetric pipe. **The double-diffusive phenomenon observed in density-stratified systems in the context of thermohaline convection is briefly discussed below [16].**

Imagine in the ocean, a layer of fresh water (lighter) lying above a layer of salty water (heavier), which is expected to be stable. And indeed it is, except when another scalar is added in to the system. Now, the other scalar could be heat (common in the ocean). Now consider a warm salty layer of water which lies above a cold, fresh layer, and with a net density less than that of the bottom layer. This situation at first glance is stable. However, since heat diffuses away faster, we will soon have a salty layer lying above a fresh water layer, at nearly the same temperature. This, now, is top-heavy and unstable, and fingers of salty water will start descending into the fresh layer. This is known as fingering instability. Now, let us consider the reverse, e.g. when the original salty, warmer and

denser ocean water laying below the cold fresh water from a river. If a blob of cold fresh water is displaced downwards into the salty and warmer ocean water, being lighter than its surroundings, it will feel a buoyancy force pushing it back up, namely a stabilising effect. However, heat will diffuse away fast, and by the time the river water comes back to its original place, it will be warmer than it was before, and so lighter than its surroundings. It will therefore overshoot its original position, and this happens repeatedly as the amplitude of the oscillation increases. This is termed the oscillatory mode of DD instability.

The viscosity-stratified single-component systems have been studied by many authors [17–26]. Several configurations, such as core-annular, three-layer and displacement flows are considered in these studies. The relevant finding from these studies are summarized as follows. In three-layer planar channel flow, decreasing the viscosity towards the wall has a significant stabilising influence. As expected, the stabilising effects accentuated with the decrease in viscosity contrast of the fluids occupying the near-wall and centre-line regions. On the other hand, increasing the viscosity of the fluid toward the walls destabilises the three-layer channel flow. In such unstable configurations, Sahu et al. [24] found the presence of absolute instability under certain parameter ranges by conducting a linear stability analysis, which in turn takes the flow towards a transitional state via nonlinear mechanism. On the other hand, core-annular pipe flow is different. For higher viscosity ratios, the flow becomes unstable even when the less-viscous fluid is at the wall [22]. By conducting a linear stability analysis, Govindarajan and co-workers [10, 27] observed a new instability mode due to double-diffusive phenomenon in a three-layer planar channel flow with the less viscous fluid occupying the near wall regions. **The mixing in single-component viscosity-stratified flow in porous media has been investigated by Jha et al. [28, 29].** The readers are referred to the recent review articles [6, 11], which discuss the instability in viscosity stratified flows.

As the above brief review shows, all the previous work carried out on double-diffusive effect has so far been for planar channel, although cylindrical geometries are frequently encountered in industrial applications. The present study is an extension of Mishra et al. [9] and Sahu [8] to investigate the double-diffusive effect for displacement flow through an axisymmetric pipe. **Through a series of direct numerical simulations, they investigated the instabilities due to double-diffusive effect in pressure-driven**

displacement flow of a less viscous fluid by a highly viscous fluid, which is injected at the inlet of a planar channel. As discussed above this is a stable configuration in the context of single-component flows. The effects of diffusivity ratio of the faster and slower diffusing species have been investigated and **various instability patterns were found** once the finger of the highly viscous fluid penetrates inside the channel.

The rest of this paper is organised as follows. The formulation and equations governing the flow are presented in section 2. The results are discussed in section 3. Concluding remarks are given in section 4.

2. Formulation

We consider pressure-driven displacement flow of one fluid (fluid '2') by another one (fluid '1') in an axisymmetric pipe of diameter D and length L, as shown in Fig. 1. **Both the fluids have the same density, and** are assumed to be incompressible and Newtonian, with dynamic viscosities μ_1 and μ_2, respectively. The viscosity of the invading fluid is higher than that of the resident fluid ($\mu_1 > \mu_2$). This is a stable configuration in the context of single-component systems [3, 6], as discussed in section 1. **Here, the resident (fluid '2') and invading (fluid '1') fluids consist of the same solvent, but contain two species (S and F) diffusing at different rates, wherein S and F represent the slower and faster diffusing species, respectively.** $\mathcal{D}_f$ and $\mathcal{D}_s$ are the diffusivities of the faster and slower diffusing species, respectively, such that $\delta = \mathcal{D}_f/\mathcal{D}_s > 1$ (by definition). The pipe wall is assumed to be rigid and impermeable, with inlet and outlet at $x = 0$ and $x = L$, respectively. **In order to minimise the entry effects, at the starting of the simulation the invading fluid is filled upto $x = D$ inside the pipe.** The invading fluid (fluid '1' having species S and F in quantity S_1 and F_1) is injected at the inlet of the pipe with an average velocity, $V(\equiv Q/A)$, where Q and $A\,(\equiv \pi D^2/4)$ denote the flow rate and cross-sectional area of the pipe, respectively. The resident fluid (fluid '2' having species S and F in quantity S_2 and F_2) is initially kept stationary inside the pipe ($D \leq x \leq L$). The length of the pipe is considered to be $100D$.

The viscosity, μ is modelled using the following viscosity-concentration relationship [4, 10, 30, 31] for liquid systems:

$$\mu = \mu_1 \exp\left[R_s\left(\frac{S - S_1}{S_2 - S_1}\right) + R_f\left(\frac{F - F_1}{F_2 - F_1}\right)\right], \tag{1}$$

where $R_s\,(\equiv (S_2 - S_1)d(\ln\mu)/dS)$ and $R_f\,(\equiv (F_2 - F_1)d(\ln\mu)/dF)$ are the log-mobility ratios of species S and F, respectively. We have used this viscosity-concentration relationship as the objective of this study is to compare the flow dynamics with double-diffusive effects in an axisymmetric pipe with those observed in an two-dimensional channel [8, 9], where this formulation was used.

An axisymmetric cylindrical coordinate system (r, x) is used to formulate the problem, where r and x denote the radial and axial coordinates, respectively. The flow dynamics is governed by the continuity and the Navier-Stokes equations coupled to the convective-diffusion equations of both species through concentration-dependent viscosity. The following scaling is employed in order to render the governing equations dimensionless:

$$(r, x) = D\,(\widetilde{r}, \widetilde{x})\,,\ t = \frac{D}{V}\widetilde{t},\ (u, v) = V(\widetilde{u}, \widetilde{v}),\ p = \rho V^2 \widetilde{p},$$
$$\mu = \widetilde{\mu}\mu_1,\ \widetilde{s} = \frac{S - S_1}{S_2 - S_1},\ \widetilde{f} = \frac{F - F_1}{F_2 - F_1}, \tag{2}$$

where the tildes designate dimensionless quantities. After dropping tildes, the dimensionless governing equations are given by

$$\nabla \cdot \mathbf{u} = 0, \tag{3}$$
$$\frac{\partial \mathbf{u}}{\partial t} + \mathbf{u} \cdot \nabla \mathbf{u} = -\nabla p + \frac{1}{\mathrm{Re}} \nabla \cdot \left[\mu(\nabla \mathbf{u} + \nabla \mathbf{u}^T)\right], \tag{4}$$
$$\frac{\partial s}{\partial t} + \mathbf{u} \cdot \nabla s = \frac{1}{\mathrm{ReSc}} \nabla^2 s, \tag{5}$$
$$\frac{\partial f}{\partial t} + \mathbf{u} \cdot \nabla f = \frac{\delta}{\mathrm{ReSc}} \nabla^2 f, \tag{6}$$

where $\mathbf{u}(u, v)$ represents axisymmetric velocity field, wherein u and v are the velocity components in the axial and radial directions, respectively; p denotes the pressure field; t is the time. Here $\mathrm{Re}(\equiv \rho V D/\mu_1)$ and $\mathrm{Sc}(\equiv \mu_1/\rho \mathcal{D}_s)$ denote Reynolds number and Schmidt number, respectively.

The dimensionless viscosity has the following dependence on f and s:

$$\mu = \exp\left(R_s s + R_f f\right), \tag{7}$$

such that $R_s + R_f < 0$ represents the situation considered here, where the invading fluid is more viscous than the resident fluid.

By setting either $R_f = 0$, or $R_s = 0$ and $\delta = 1$, we can recover the governing equations for single component systems.

Eqs. (3)-(7) are solved using no-slip, no-penetration and no-flux conditions at the pipe wall. A fully-developed velocity profile with a constant flow rate $(u_i = (0.25 - r^2)32/\pi, v_i = 0)$ **is imposed at the inlet, wherein** u_i **and** v_i **denote the axial and radial velocity components at the inlet, respectively. Neumann boundary condition for pressure is used at the outlet of the pipe.**

A finite-volume open source code, *Gerris* [32, 33] with dynamic adaptive grid refinement based on the vorticity magnitude and species concentration is used to solve Eqs. (3)-(6). A finest grid size of 0.015 (approximately) has been used for the regions which contain gradients of slower or faster diffusing species. Grids of size 0.06 (approximately) have been used to resolve the vortical regions inside the domain. We refer the readers to Tripathi et al. [33–35] for detailed description of the numerical method used in this study. The present grid size distribution was found to yield grid independent results for the onset of instability and other flow features. In order to validate our code, we have simulated displacement of one fluid by another in a two-dimensional planar channel for the same parameter values considered by Mishra et al. [9]. The spatio-temporal evolution of s contours for three values of δ is presented in Fig. 2. It can be seen that as expected $\delta = 1$ (single-component) is a stable configuration, but for $\delta > 1$ the flow becomes unstable forming Kelvin-Helmholtz (KH) type instabilities at the mixed regions. **It is to be seen that these flow patterns are in agreement with those presented in Mishra et al. [9]. However, note that fluid '2' was filled completely inside the channel considered by Mishra et al. [9], whereas in the present study, we filled fluid '2' in the region** $H \leq x \leq L$ **of the channel in order to minimise the entry effect, where** H **is the height of the channel. Due to this there is a small difference in the flow patterns observed in the present study with those reported by Mishra et al. [9].** In addition, the solver has been validated extensively for several interfacial flow problems [33–35], which have been excluded from here for brevity.

In the present study, we have extended the work of Sahu and co-workers [8, 9] to investigate the effects of double diffusion associated with the displacement flow of a less viscous fluid by a highly viscous one in an axisymmetric pipe. This is a parametrically rich problem, with several dimensionless numbers, such as Re, Sc, R_s, R_f and δ influencing the

flow dynamics. The effects of these dimensionless variables are discussed below.

3. Results and discussion

3.1. Effects of δ

We begin the presentation of our results by investigating the effects of δ on the flow dynamics in Fig. 3(a)-(d), where spatio-temporal evolution of s field has been plotted for $\delta = 1$, 2.5, 5, and 10, respectively. The rest of the parameter values used to generate this figure are Re = 100, Sc = 100, $R_s = 3$ and $R_f = -3.6$. Here $R_s + R_f < 0$, but $R_s > 0$ and $R_f < 0$, which corresponds to a situation when a highly viscous fluid displaces a less viscous fluid, and the slower and faster diffusing species have destabilising and stabilising influences, respectively. **For instance, in this case the slower and faster diffusing species could be sugar and temperature, respectively.** It can be seen that, as expected, for $\delta = 1$ the flow dynamics is stable, and a "pure-Poiseuille-diffusive" flow occurs as the finger penetrates inside the pipe. It can be seen that the KH type instabilities appear for $\delta > 1$. The intensity of instability increases with an increase in the value of δ. **For this set of parameter values, we observe that $\delta \approx 2.5$ corresponds to the onset for the instability, which can be seen in the contours of s.** Close inspection of Fig. 3(b) reveals that a spike like structure appears at the tip of the finger at later times ($t \geq 40$). **For higher values of δ, the KH type instability becomes catastrophic. Roll-up structures become apparent at earlier times and have increasingly greater intensity as time progresses.** Comparison of contours of s for $\delta = 10$ observed in **an axisymmetric pipe** (Fig. 3(d)) with those seen in a two-dimensional planar channel (Fig. 2(d)) divulge that the mushroom-like structures which are clearly visible in **a planar** channel do not appear in case of axisymmetric pipe, **and the intensity of instability is greater for the case of a two-dimensional planar channel. Also DD convection affects pipe flow for much smaller value of δ than the channel case. It can be seen in panel (b) of Figs. 2 and 3 that the flow in a two-dimensional channel is fairly stable for $\delta = 2.5$, but the instability already appears in case of an axisymmetric pipe for the same value of δ. Close inspection of Figs. 2 and 3 also reveals that the mixing in a planar channel is dominated by instabilities, where as in a pipe it is mainly dominated by diffusion mechanism. Inspection**

of results presented Fig. 2 (two-dimensional channel) and Fig. 3 (axisymmetric pipe) reveals that the speed of the finger in a pipe is higher than that observed in a planar channel for the same set of parameter values. This is also evident in Fig. 4, where the time evolution of location of the tip of the finger in a two-dimensional channel and an axisymmetric pipe are presented for different values of δ. We also observed in Fig. 4 that increasing δ increases the speed of the finger for both the channel and pipe cases.

The spatio-temporal evolution of viscosity field for different values of δ is presented in Fig. 5 for the same parameter values used to generate Fig. 3. For $\delta = 1$, the viscosity in the mixed region decreases monotonically in the positive axial direction, whereas for $\delta > 1$ the viscosity undergoes a non-monotonic distribution in the axial direction due to the double-diffusive effect. In addition to this, for $\delta > 1$ a highly viscous stenosis region forms near the wall of the pipe. The value of viscosity of the fluid in the stenosis region increases with an increase in the value of δ. This phenomenon was first observed by Taylor [36] for single-component flows. The non-monotonic viscosity distribution in the axial direction and the highly viscous stenosis formation near the wall of the pipe provide a favourable condition for the instability to grow [6], **leading to the amplification of instabilities for increasing values of δ.**

The radial variation of viscosity at a later dimensionless time ($t = 50$) for different axial locations are plotted in Fig. 6(a)-(d) for $\delta = 1$, 2.5, 5, and 10, respectively. It can be seen that a core-annular configuration is formed with the less viscous fluid in the annular region for $\delta = 1$. The viscosity in this case decreases monotonically in the radial direction at all x locations. This is a stable configuration, as shown by Govindarajan and co-workers via linear stability analyses [6, 17]. For $\delta > 1$ the viscosity profiles encounter minima at intermediate radial locations (in the mixed region) for all axial locations, with the annular region occupied with highly viscous fluid, thus making the flow unstable. Close inspection of Fig. 6(b)-(d) also reveals that the value of the near-wall viscosity increases with an increase in δ value, **thereby making the flow more unstable**. The effect of the log-mobility ratio of the slower diffusing species, R_s is investigated next.

3.2. Effects of R_s

The spatio-temporal evolutions of the concentration field of the slower diffusing species are presented for $R_s = 0.5$, 1.5, 2 and 3 in Fig. 7(a), (b),

(c) and (d), respectively. The rest of the parameter values are Re = 100, Sc = 100, $\delta = 10$ and $R_f = -3.6$. **Again** the slower and faster diffusing species have destabilising and stabilising influences, respectively. In addition to this, $R_s + R_f < 0$, thus a highly viscous fluid is displacing a less viscous one inside the pipe. For $R_s = 0.5$, the viscosity of the invading fluid is approximately 22.2 times higher than that of the resident fluid. The value of δ ($\delta = 10$) considered in this case is not high enough to create instabilities. In this case, a finger with a 'blunt' nose penetrates inside the pipe as the time progresses. With an increase in the value of R_s, the viscosity ratios between the invading and resident fluids decreases. For $R_s = 1.5$, the nose of the finger becomes sharper, and the onset of instabilities occurs at $R_s = 1.5$ for the set of parameter values considered. Further increase in the value of R_s leads to KH type instabilities at the mixed region separating the fluids. This behaviour is also evident in Figs. 8 and 9. The appearance of highly viscous stenosis region near the wall, which is the source for these instabilities is not significant enough for $R_s = 0.5$, but starts to dominate the instability dynamics for $R_s \geq 1.5$ for this set of parameter values.

The axially averaged viscosity (μ_x) versus r, and radially averaged viscosity (μ_r) versus x profiles are plotted at $t = 30$ in Fig. 9(a) and (b), respectively. It can be seen in Fig. 9(a) that for $R_s \geq 1.5$, the dynamics due to the double-diffusive effect creates a core-annular configuration, with highly viscous fluid in the annular region. The non-monotonic trend of the radially averaged viscosity profiles are also apparent for $R_s \geq 1.5$ in Fig. 9(b), which implies that although initially a highly viscous fluid was displacing a less viscous fluid, at later times due to the double-diffusive effects a situation is created locally, wherein a less viscous fluid displaces a highly viscous one. This phenomenon makes the flow unstable [3].

3.3. Effects of R_f

We then investigate the effects of changes to the log-mobility ratio of the faster diffusing species. In Fig. 9(a), (b) and (c), we plot the spatio-temporal evolution of s for R_f = -1, -3 and -5 respectively. The rest of the parameter values are Re = 100, Sc = 100, $\delta =$ 10 and $R_s = 2$. **The results presented in Fig. 9(a) are characteristic of a situation** when a less viscous fluid displaces a highly viscous fluid occupying the pipe initially (i.e. $R_s + R_f > 0$; unstable configuration even for single-component systems). It can be seen that a cap-type instability appears at the tip of the finger, with a 'blunt' nose. The results presented

in Fig. 10(b) and (c) are stable in the context of single-component systems; however, become unstable due to differential diffusivity of the slower and faster diffusing species ($\delta = 10$). Decreasing the value of R_f by keeping R_s constant decreases the double-diffusive instability. **It can be seen in Fig. 10(a) that, for t=30, the viscosity contrast of the annular to the core fluids decreases with R_f. Such effect was also observed for all later times considered (not shown).** Also the peak of the radially averaged viscosity near the entrance region decreases with a reduction in the value of R_f, and thereby stabilising the flow dynamics.

3.4. Effects of Re

Finally, in Fig. 12, the effects of Re are shown for Sc = 100, $\delta = 10$, $R_s = 3$, and $R_f = -3.6$. It can be seen that flow becomes vigorously unstable with an increase in the value of Re. **This behaviour is not surprising as the destabilising behaviour of Reynolds number can be observed in many shear flows. Close inspection of this figure also reveals that the nose of the finger becomes increasingly sharp as** Re **is increased, but surprisingly becomes blunt for** Re = 1000**. Increasing Reynolds number by keeping the Schmidt number fixed also implies that the Péclet number** ($ReSc$)**, which characterises diffusion, is increased. It can be seen in Fig. 12 that the mixing due to diffusion decreases with an increase in the value of** Re**, which increases (decreases) the Péclet number (diffusive mixing). Comparison of the spatio-temporal variation of** s **contours shown in Fig. 12 for an axisymmetric pipe with those of Mishra et al. [9] for a two-dimensional channel reveals that the present flow is more unstable than that observed in a channel.**

4. Concluding remarks

In this paper, the pressure-driven displacement flow, focusing on the situation when the invading fluid is more viscous than the resident fluid (classically a stable configuration in the context of single-component systems), is investigated in an axisymmetric pipe, using an open source code, *Gerris* based on finite-volume approach. The fluids considered in the present study have the same density, but different viscosity. The viscosity stratification is achieved through the addition of two solute species diffusing at different rates. The viscosity is modelled as an exponential function of the concentration of

both the species. An extensive parametric study has been conducted, and the influences of diffusivity ratio, log-mobility ratios of the slower and faster diffusing species, and Reynolds number on the flow dynamics have been investigated. Our results demonstrate the presence of instability patterns due to double-diffusive effect, which are qualitatively different from those observed in **a planar** channel and also in situations when a less viscous fluid displaces a highly viscous fluid. We found that increasing the values of δ and R_s, keeping R_f fixed, makes the flow increasingly unstable. Similar trend is observed when the Reynolds number is increased. We observe a 'blunt' nose of the penetrating finger for lower value of R_s, which becomes sharper with increasing R_s value. It is demonstrated that although initially a highly viscous fluid displaces a less viscous one, at later times, a local situation is created due to the double-diffusive phenomenon, wherein less viscous fluid becomes the displacing fluid. Also, at later times, the viscosity of the fluid in annular region becomes more viscous as compared to that in the core of the pipe, which starts the instability observed in the present study.

[1] G. M. Homsy, Viscous fingering in porous media, Ann. Rev. Fluid Mech. 19 (1987) 271–311.

[2] R. Chouke, P. Van Meurs, C. Van Der Pol, The instability of slow, immiscible, viscous liquid-liquid displacements in permeable media, Trans. AIME 216 (1959) 188–194.

[3] P. Saffman, G. Taylor, The penetration of a finger into a porous medium in a Hele-Shaw cell containing a more viscous liquid, Proc. Roy. Soc. Lond. A 245 (1958) 312–329.

[4] C. T. Tan, G. M. Homsy, Stability of miscible displacements in porous media: Rectilinear flow, Phys. Fluid 29 (1986) 3549–3556.

[5] K. C. Sahu, O. K. Matar, Stability of plane channel flow with viscous heating, J. Fluids Eng. 132 (2010) 011202.

[6] R. Govindarajan, K. C. Sahu, Instabilities in viscosity-stratified flows, Ann. Rev. Fluid Mech. 46 (2014) 331–353.

[7] M. Mishra, P. M. J. Trevelyan, C. Almarcha, A. D. Wit, Influence of double diffusive effects and miscible viscous fingering, Physical review letters 105 (2010) 204501.

[8] K. C. Sahu, Double diffusive effects on pressure-driven miscible channel flow: Influence of variable diffusivity, Int. J. Multiphase Flow 55 (2013) 24–31.

[9] M. Mishra, A. De Wit, K. C. Sahu, Double diffusive effects on pressure-driven miscible displacement flows in a channel, J. Fluid Mech. 712 (2012) 579–597.

[10] K. C. Sahu, R. Govindarajan, Linear stability of double-diffusive two-fluid channel flow, J. Fluid Mech. 687 (2011) 529–539.

[11] K. C. Sahu, A review of double-diffusive instability in viscosity stratified flows, Proc Indian Natn Sci Acad 80 (3) (2014) 513–514.

[12] S. Ghosh, R. Usha, K. C. Sahu, Double-diffusive two-fluid flow in a slippery channel: A linear stability analysis, Phys. Fluids. 26 (2014) 015412.

[13] S. Ghosh, R. Usha, K. C. Sahu, 'linear stability anlysis of miscble two-fluid flow in a channel with velocity slip at the walls, Phys. Fluids. 26 (2014) 014107.

[14] J. S. Turner, Double-diffusive phenomena, Annual Review of Fluid Mechanics 6 (1974) 37–54.

[15] K. C. Sahu, R. Govindarajan, Stability of flow through a slowly diverging pipe, J. Fluid Mech. 531 (2005) 325–534.

[16] T. Radko, M. E. Stern, Finescale instabilities of the double-diffusive shear flow, J. Phys. Oceanogr. 41 (2011) 571–585.

[17] B. T. Ranganathan, R. Govindarajan, Stabilisation and destabilisation of channel flow by location of viscosity-stratified fluid layer, Phys. Fluids. 13(1) (2001) 1–3.

[18] P. Ern, F. Charru, P. Luchini, Stability analysis of a shear flow with strongly stratified viscosity, J. Fluid Mech. 496 (2003) 295–312.

[19] E. J. Hinch, A note on the mechanism of the instability at the interface between two shearing fluids, J. Fluid Mech. 144 (1984) 463–465.

[20] M. J. South, A. P. Hooper, Linear growth in two-fluid plane Poiseuille flow, J. Fluid Mech. 381 (1999) 121–139.

[21] S. V. Malik, A. P. Hooper, Linear stability and energy growth of viscosity stratified flows, Phys. Fluids 17 (2005) 024101.

[22] B. Selvam, S. Merk, R. Govindarajan, E. Meiburg, Stability of miscible core-annular flows with viscosity stratification, J. Fluid Mech. 592 (2007) 23–49.

[23] B. Selvam, L. Talon, L. Lesshafft, E. Meiburg, Convective/absolute instability in miscible core-annular flow. part 2. numerical simulations and nonlinear global modes, J. Fluid Mech. 618 (2009) 323–348.

[24] K. C. Sahu, H. Ding, P. Valluri, O. K. Matar, Linear stability analysis and numerical simulation of miscible channel flows, Phys. Fluids 21 (2009) 042104.

[25] K. C. Sahu, H. Ding, O. K. Matar, Numerical simulation of non-isothermal pressure-driven miscible channel flow with viscous heating, Chem. Engg. Sci. 65 (2010) 3260–3267.

[26] D. D. Joseph, R. Bai, K. P. Chen, Y. Y. Renardy, Core-annular flows, Ann. Rev. Fluid Mech. 29 (1997) 65–90.

[27] K. C. Sahu, R. Govindarajan, Spatio-temporal linear stability of double-diffusive two-fluid channel flow, Phys. Fluids 24 (2012) 054103.

[28] B. Jha, L. Cueto-Felgueroso, R. Juanes, Quantifying mixing in viscously unstable porous media flows, Phys. Rev. E. 84 (2011) 066312.

[29] B. Jha, L. Cueto-Felgueroso, R. Juanes, Fluid mixing from viscous fingering, Phys. Rev. Lett. 106 (2011) 194502.

[30] S. Arrhenius, über die inner reibung verdünnter wässeriger lösungen, Z. Phys. Chem. 1 (1887) 285–298.

[31] C.-Y. Chen, E. Meiburg, Miscible displacement in capillary tubes. part 2. numerical simulations, J. Fluid Mech. 326 (1996) 57.

[32] S. Popinet, Gerris: a tree-based adaptive solver for the incompressible euler equations in complex geometries, J. Comput. Phys 190 (2003) 572–600.

[33] M. K. Tripathi, K. C. Sahu, R. Govindarajan, Why a falling drop does not in general behave like a rising bubble, Sci. Rep. 4 (2014) 4771.

[34] M. K. Tripathi, K. C. Sahu, G. Karapetsas, K. Sefiane, O. K. Matar, Non-isothermal bubble rise: non-monotonic dependence of surface tension on temperature, J. Fluid Mech. 763 (2015) 82–108.

[35] M. K. Tripathi, K. C. Sahu, R. Govindarajan, Dynamics of an initially spherical bubble rising in quiescent liquid, Nat. Commun. 6 (2015) 6268.

[36] G. I. Taylor, Deposition of viscous fluid on the wall of a tube, J. Fluid Mech. 10 (1961) 161.

List of figures

Fig. 1: The schematic (not to scale) showing the initial flow configuration. The portions of the pipe $0 \leq x \leq D$ and $D \leq x \leq L$ are filled with fluid '1' and fluid '2', respectively. The aspect ratio of the pipe, L/D is 100.

Fig. 2: **Spatio-temporal evolution of the concentration field of species s at different times in a two-dimensional planar channel (from top to bottom, $t = 20$, 40, 50 and 75) for (a) $\delta = 1$, (b) $\delta = 2.5$, (c) $\delta = 5$ and (d) $\delta = 10$. The rest of the parameter values are** $\mathrm{Re} = 100$, $\mathrm{Sc} = 100$, $R_s = 3$ **and** $R_f = -3.6$. **The flow dynamics obtained using the present solver is very similar to those observed in Mishra et al. [9].**

Fig. 3: Spatio-temporal evolution of the concentration field of species s at successive times (from top to bottom, $t = 20$, 40, 50 and 75) for (a) $\delta = 1$, (b) $\delta = 2.5$, (c) $\delta = 5$ and (d) $\delta = 10$. The rest of the parameter values are $\mathrm{Re} = 100$, $\mathrm{Sc} = 100$, $R_s = 3$ and $R_f = -3.6$. **The centerline of the pipe is located at the middle of each panel.**

Fig. 4: **The temporal evolution of the position of the leading front separating the two fluids, x_{tip} for different values of δ: Dashed lines: two dimensional channel, solid lines: axisymmetric pipe. The rest of the parameter values are the same as those used to generate Fig. 3. The dashed and solid lines without symbols represent analytical solutions obtained assuming a plug flow displacement in the two-dimensional channel and the axisymmetric pipe, respectively.**

Fig. 5: Spatio-temporal evolution of the viscosity field at successive times (from top to bottom, $t = 20$, 40, 50 and 75) for (a) $\delta = 1$, (b) $\delta = 2.5$, (c) $\delta = 5$ and (d) $\delta = 10$. The rest of the parameter values are $\mathrm{Re} = 100$, $\mathrm{Sc} = 100$, $R_s = 3$ and $R_f = -3.6$. **The centerline of the pipe is located at the middle of each panel.**

Fig. 6: Variation of viscosity at $t = 50$ in the radial direction at different axial locations for (a) $\delta = 1$, (b) $\delta = 2.5$, (c) $\delta = 5$ and (d) $\delta = 10$. The rest of the parameter values are $\mathrm{Re} = 100$, $\mathrm{Sc} = 100$, $R_s = 3$ and $R_f = -3.6$.

Fig. 7: Spatio-temporal evolution of the concentration field of species s at successive times (from top to bottom, t = 20, 40, 50 and 75) for (a) $R_s = 0.5$, (b) $R_s = 1.5$, (c)$R_s = 2$ and (d) $R_s = 3$. The rest of the parameter values are Re = 100, Sc = 100, $\delta = 10$ and $R_f = -3.6$. **The centerline of the pipe is located at the middle of each panel.**

Fig. 8: Spatio-temporal evolution of the viscosity field at successive times (from top to bottom, t = 20, 40, 50 and 75) for for (a) $R_s = 0.5$, (b) $R_s = 1.5$, (c)$R_s = 2$ and (d) $R_s = 3$. The rest of the parameter values are Re = 100, Sc = 100, $\delta = 10$ and $R_f = -3.6$. **The centerline of the pipe is located at the middle of each panel.**

Fig 9: **Variation of (a) axially averaged viscosity** ($\mu_x \equiv \frac{D}{L}\int_0^{L/D} \mu dx$) **versus** r**, (b) radially averaged viscosity** ($\mu_r \equiv \frac{8}{D^2}\int_0^{D/2} \mu r dr$) **versus** x **for different values of** R_s**, at** $t = 30$ **for** Re = 100**,** Sc = 100**,** $\delta = 10$ **and** $R_f = -3.6$**.**

Fig. 10: Spatio-temporal evolution of the concentration field of species s at successive times (from top to bottom, t = 20, 40, 50 and 75) for (a) $R_f = -1$, (b) $R_f = -3$ and (c) $R_f = -5$. The rest of the parameter values are Re = 100, Sc = 100, $\delta = 10$ and $R_s = 2$. **The centerline of the pipe is located at the middle of each panel.**

Fig. 11: **Variation of (a) axially averaged viscosity** ($\mu_x \equiv \frac{D}{L}\int_0^{L/D} \mu dx$) **versus** r**, (b) radially averaged viscosity** ($\mu_r \equiv \frac{8}{D^2}\int_0^{D/2} \mu r dr$) **versus** x **for different values of** R_f**, at** $t = 30$ **for** Re = 100**,** Sc = 100**,** $\delta = 10$ **and** $R_s = 2$**.**

Fig. 12: Spatio-temporal evolution of the concentration field of species s at successive times (from top to bottom, t = 20, 40, 50 and 75) for (a) Re = 50, (b) Re = 500 and (c) Re = 1000. The rest of the parameter values are Sc = 100, $\delta = 10$, $R_s = 3$, and $R_f = -3.6$. **The centerline of the pipe is located at the middle of each panel.**

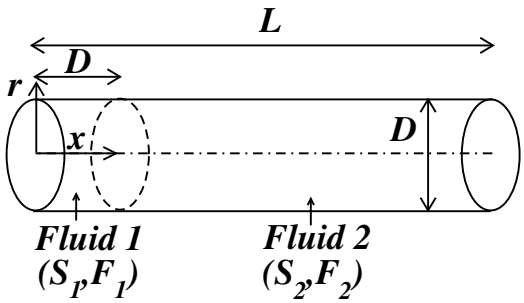

Figure 1: **The schematic (not to scale) showing the initial flow configuration. The portions of the pipe $0 \leq x \leq D$ and $D \leq x \leq L$ are filled with fluid '1' and fluid '2', respectively. The aspect ratio of the pipe, L/D is 100.**

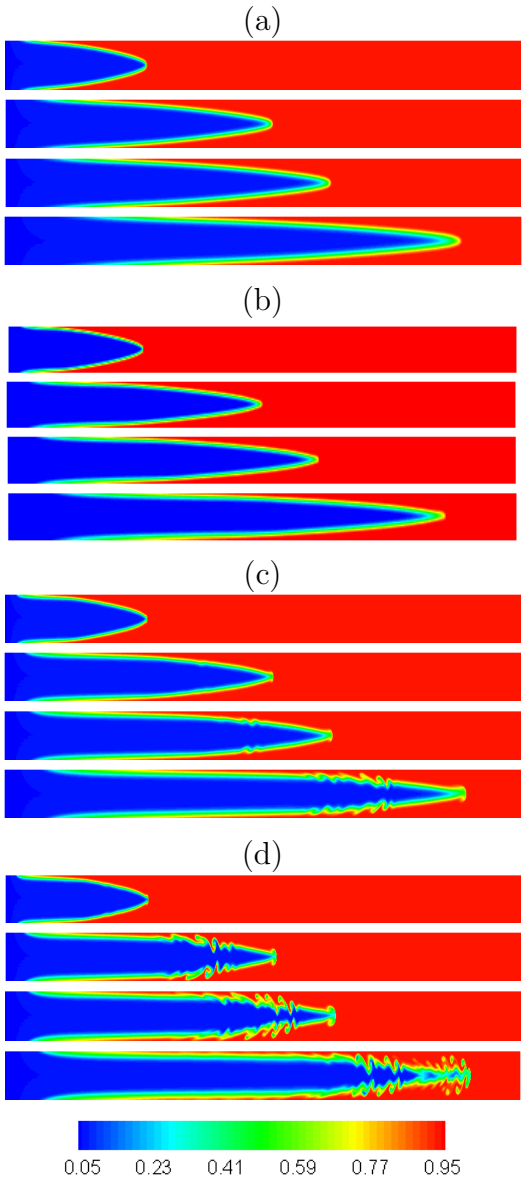

Figure 2: **Spatio-temporal evolution of the concentration field of species s at different times in a two-dimensional planar channel (from top to bottom, $t = 20$, 40, 50 and 75) for (a) $\delta = 1$, (b) $\delta = 2.5$, (c) $\delta = 5$ and (d) $\delta = 10$. The rest of the parameter values are $\mathrm{Re} = 100$, $\mathrm{Sc} = 100$, $R_s = 3$ and $R_f = -3.6$. The flow dynamics obtained using the present solver is very similar to those observed in Mishra et al. [9].**

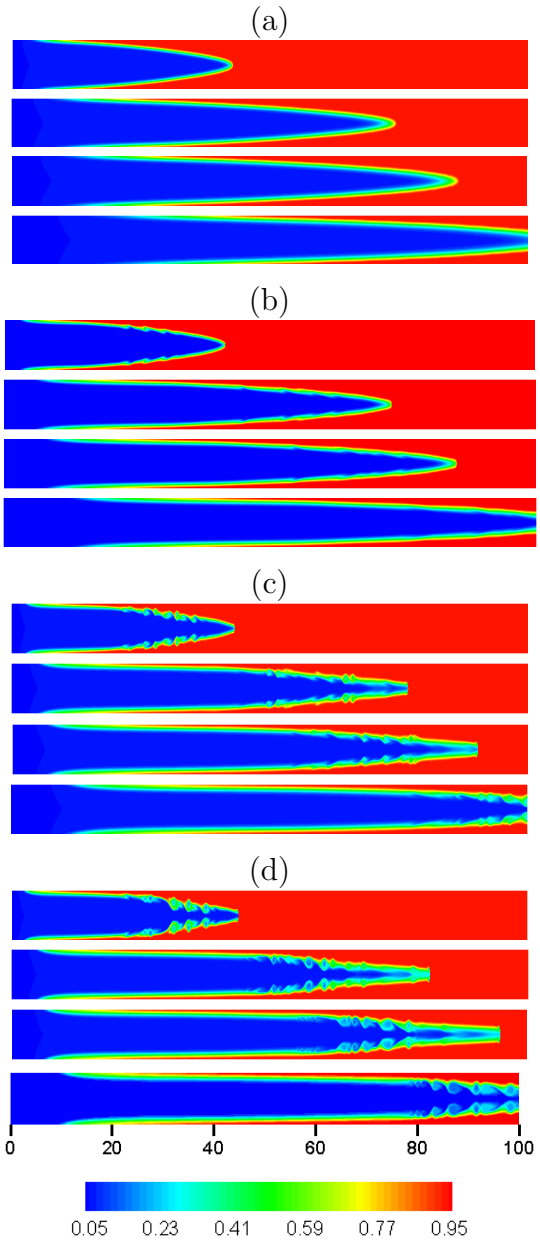

Figure 3: Spatio-temporal evolution of the concentration field of species s at successive times (from top to bottom, $t = 20$, 40, 50 and 75) for (a) $\delta = 1$, (b) $\delta = 2.5$, (c) $\delta = 5$ and (d) $\delta = 10$. The rest of the parameter values are Re $= 100$, Sc $= 100$, $R_s = 3$ and $R_f = -3.6$. **The centerline of the pipe is located at the middle of each panel.**

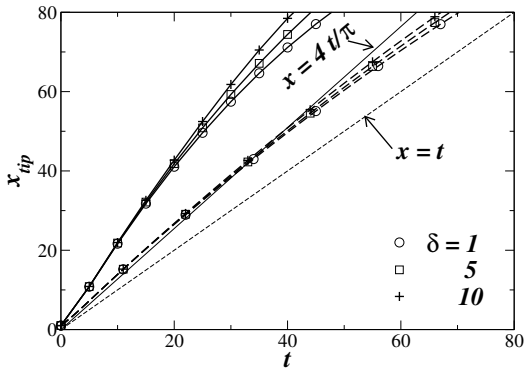

Figure 4: **The temporal evolution of the position of the leading front separating the two fluids, x_{tip} for different values of δ: Dashed lines: two dimensional channel, solid lines: axisymmetric pipe. The rest of the parameter values are the same as those used to generate Fig. 3. The dashed and solid lines without symbols represent analytical solutions obtained assuming a plug flow displacement in the two-dimensional channel and the axisymmetric pipe, respectively.**

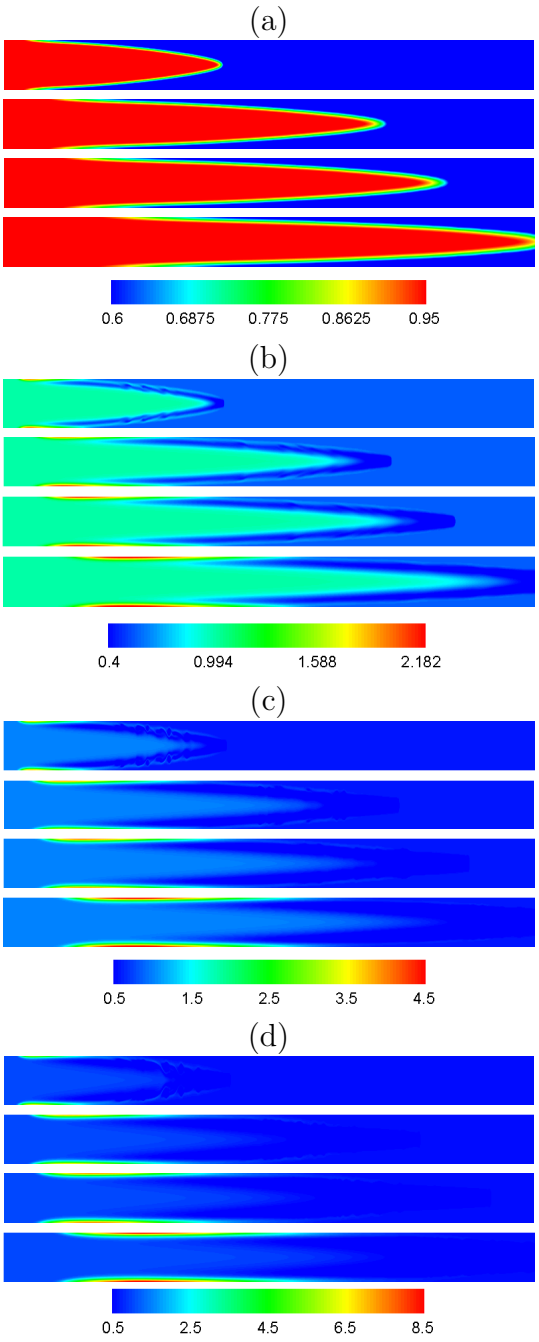

Figure 5: Spatio-temporal evolution of the viscosity field at successive times (from top to bottom, $t = 20$, 40, 50 and 75) for (a) $\delta = 1$, (b) $\delta = 2.5$, (c) $\delta = 5$ and (d) $\delta = 10$. The rest of the parameter values are Re $= 100$, Sc $= 100$, $R_s = 3$ and $R_f = -3.6$. **The centerline of the pipe is located at the middle of each panel.**

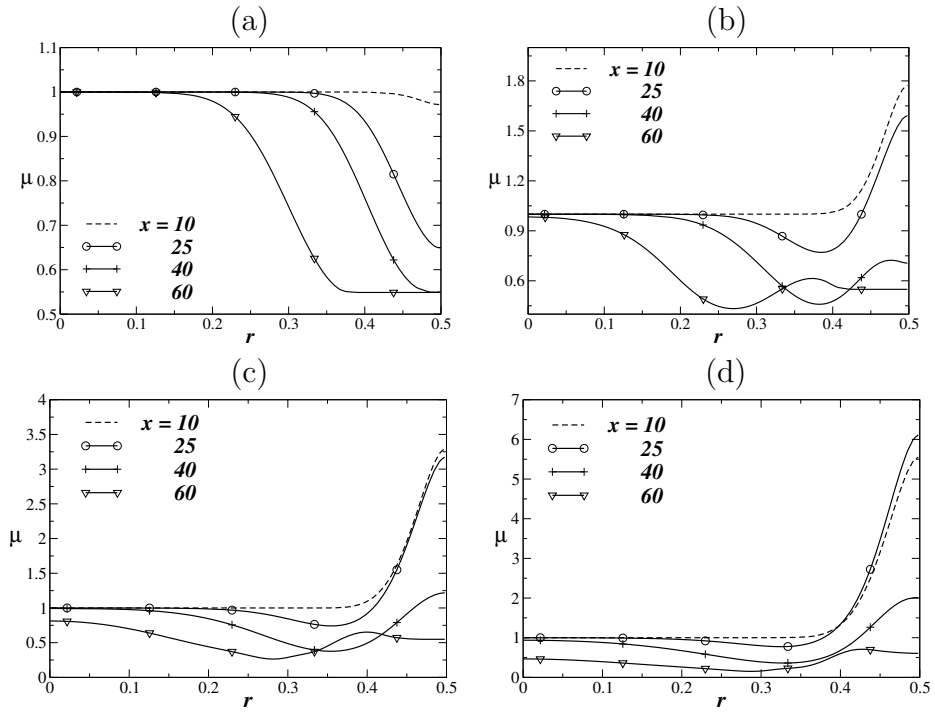

Figure 6: Variation of viscosity at $t = 50$ in the radial direction at different axial locations for (a) $\delta = 1$, (b) $\delta = 2.5$, (c) $\delta = 5$ and (d) $\delta = 10$. The rest of the parameter values are $\mathrm{Re} = 100$, $\mathrm{Sc} = 100$, $R_s = 3$ and $R_f = -3.6$.

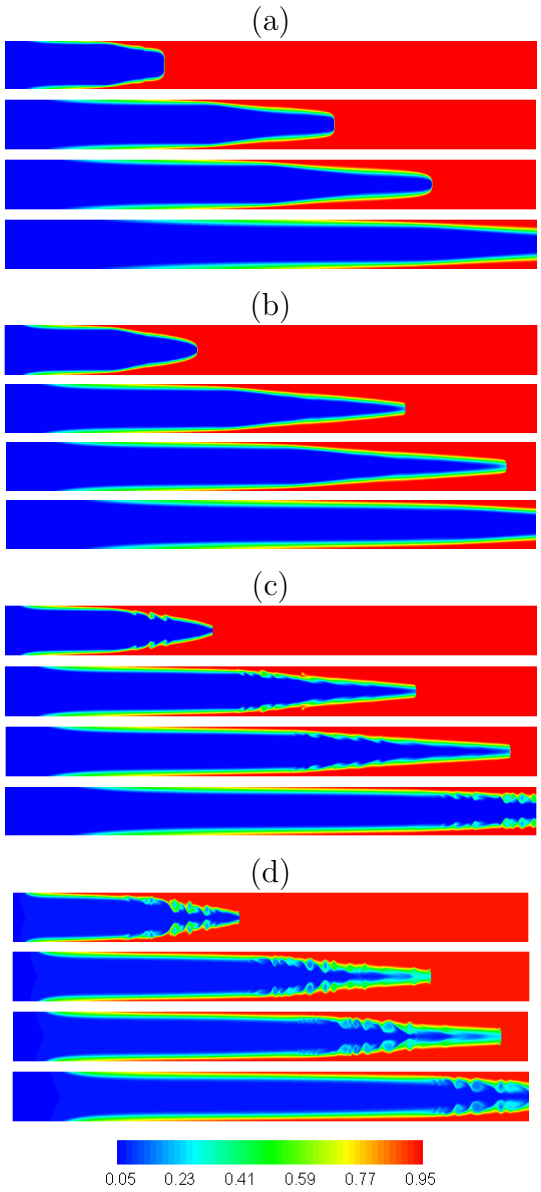

Figure 7: Spatio-temporal evolution of the concentration field of species s at successive times (from top to bottom, $t = 20$, 40, 50 and 75) for (a) $R_s = 0.5$, (b) $R_s = 1.5$, (c)$R_s = 2$ and (d) $R_s = 3$. The rest of the parameter values are Re $= 100$, Sc $= 100$, $\delta = 10$ and $R_f = -3.6$. **The centerline of the pipe is located at the middle of each panel.**

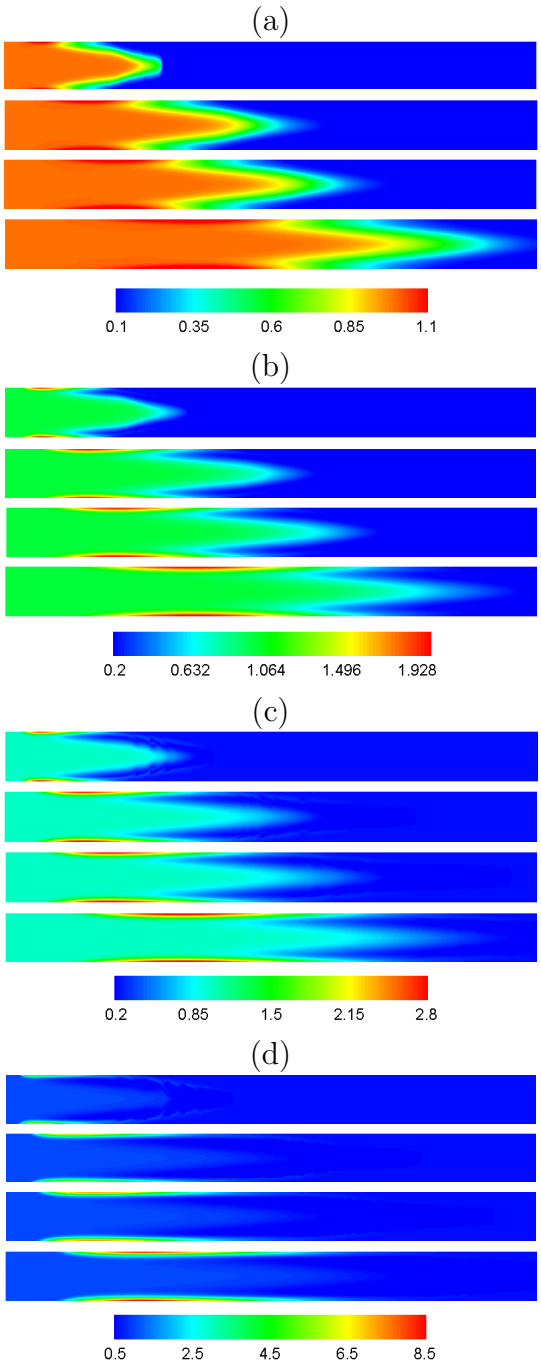

Figure 8: Spatio-temporal evolution of the viscosity field at successive times (from top to bottom, $t = 20$, 40, 50 and 75) for for (a) $R_s = 0.5$, (b) $R_s = 1.5$, (c)$R_s = 2$ and (d) $R_s = 3$. The rest of the parameter values are Re $= 100$, Sc $= 100$, $\delta = 10$ and $R_f = -3.6$. **The centerline of the pipe is located at the middle of each panel.**

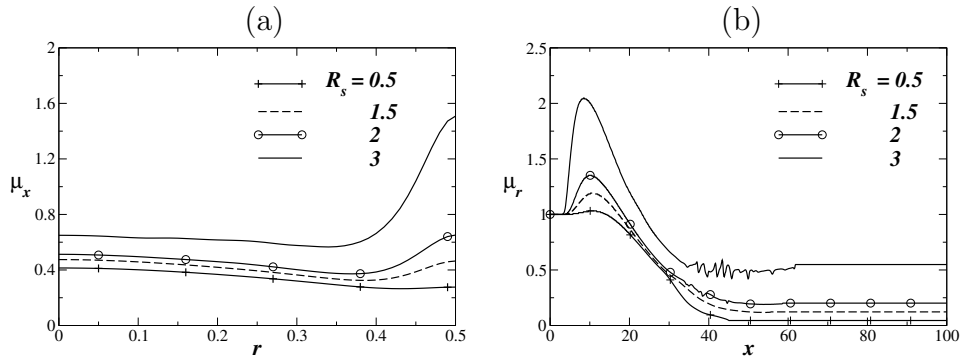

Figure 9: **Variation of (a) axially averaged viscosity** ($\mu_x \equiv \frac{D}{L}\int_0^{L/D} \mu dx$) **versus** r**, (b) radially averaged viscosity** ($\mu_r \equiv \frac{8}{D^2}\int_0^{D/2} \mu r dr$) **versus** x **for different values of** R_s**, at** $t = 30$ **for** $\mathrm{Re} = 100$**,** $\mathrm{Sc} = 100$**,** $\delta = 10$ **and** $R_f = -3.6$**.**

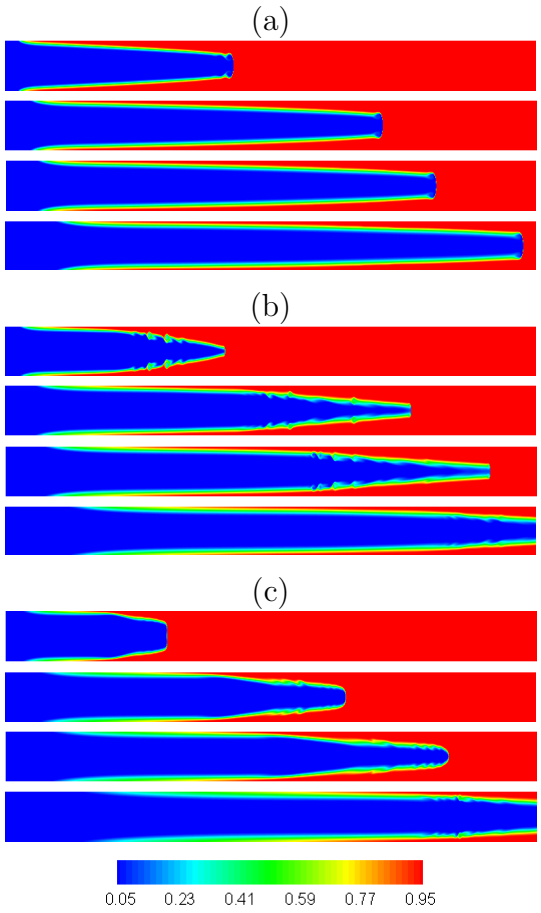

Figure 10: Spatio-temporal evolution of the concentration field of species s at successive times (from top to bottom, $t = 20$, 40, 50 and 75) for (a) $R_f = -1$, (b) $R_f = -3$ and (c) $R_f = -5$. The rest of the parameter values are Re $= 100$, Sc $= 100$, $\delta = 10$ and $R_s = 2$. **The centerline of the pipe is located at the middle of each panel.**

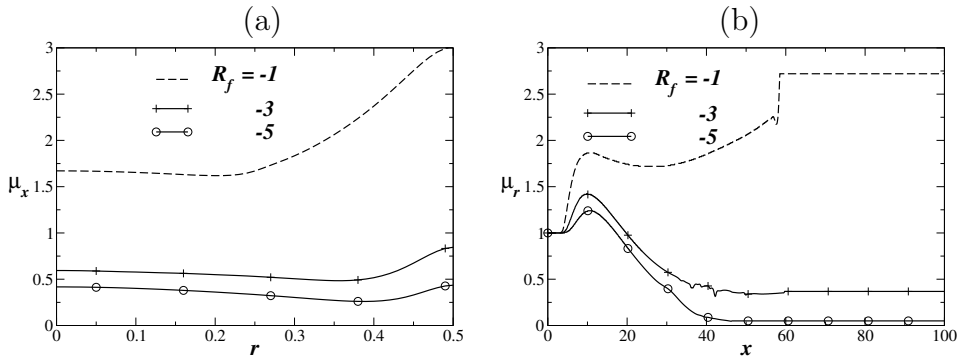

Figure 11: **Variation of (a) axially averaged viscosity** ($\mu_x \equiv \frac{D}{L}\int_0^{L/D} \mu dx$) **versus** r**, (b) radially averaged viscosity** ($\mu_r \equiv \frac{8}{D^2}\int_0^{D/2} \mu r dr$) **versus** x **for different values of** R_f**, at** $t = 30$ **for** $\mathrm{Re} = 100$**,** $\mathrm{Sc} = 100$**,** $\delta = 10$ **and** $R_s = 2$**.**

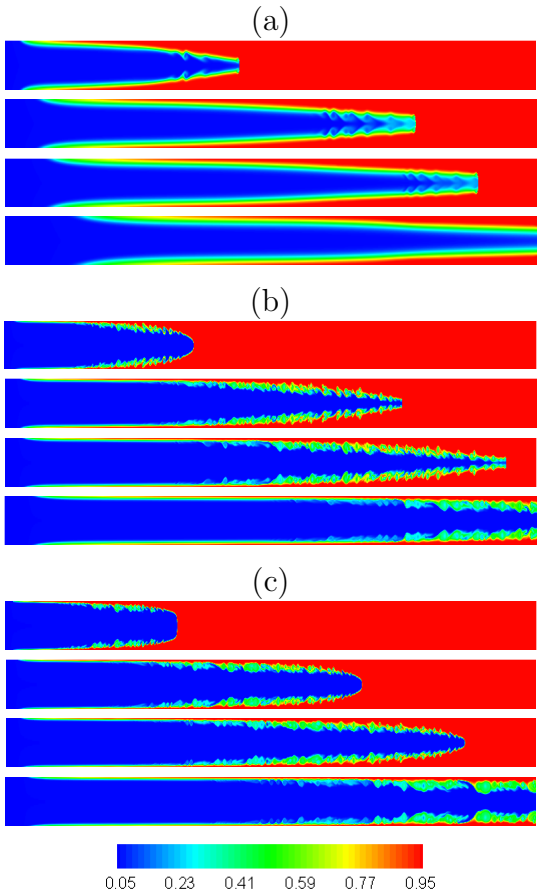

Figure 12: Spatio-temporal evolution of the concentration field of species s at successive times (from top to bottom, $t = 20$, 40, 50 and 75) for (a) Re = 50, (b) Re = 500 and (c) Re = 1000. The rest of the parameter values are Sc = 100, $\delta = 10$, $R_s = 3$, and $R_f = -3.6$. **The centerline of the pipe is located at the middle of each panel.**